

NEA HTTR LOFC Project Test#3 Benchmark Results

M3AT-24IN0603012

SEPTEMBER 2024

Robert F. Kile,
Paolo Balestra, and
Gerhard Strydom

Idaho National Laboratory



DISCLAIMER

This information was prepared as an account of work sponsored by an agency of the U.S. Government. Neither the U.S. Government nor any agency thereof, nor any of their employees, makes any warranty, expressed or implied, or assumes any legal liability or responsibility for the accuracy, completeness, or usefulness, of any information, apparatus, product, or process disclosed, or represents that its use would not infringe privately owned rights. References herein to any specific commercial product, process, or service by trade name, trade mark, manufacturer, or otherwise, does not necessarily constitute or imply its endorsement, recommendation, or favoring by the U.S. Government or any agency thereof. The views and opinions of authors expressed herein do not necessarily state or reflect those of the U.S. Government or any agency thereof.

NEA HTTR LOFC Project Test#3 Benchmark Results

M3AT-24IN0603012

**Robert F. Kile,
Paolo Balestra, and
Gerhard Strydom
Idaho National Laboratory**

September 2024

**Idaho National Laboratory
INL ART Program
Idaho Falls, Idaho 83415**

<http://www.inl.gov>

**Prepared for the
U.S. Department of Energy
Office of Nuclear Energy
Under DOE Idaho Operations Office
Contract DE-AC07-05ID14517**

Page intentionally left blank

INL ART Program

NEA HTTR LOFC Project Test#3 Benchmark Results

INL/RPT-24-80315

September 2024

Technical Reviewer: (Confirmation of mathematical accuracy, and correctness of data and appropriateness of assumptions.)



David Alan Reger
Nuclear Engineer

8/30/2024

Date

Approved by:



Michael E. Davenport
ART Project Manager

8/29/2024

Date



Travis R. Mitchell
ART Program Manager

8/30/2024

Date



Michelle T. Sharp
INL Quality Assurance

8/30/2024

Date

Page intentionally left blank

ABSTRACT

In the second half of Fiscal Year 2023, the High Temperature Engineering Test Reactor (HTTR) loss of forced cooling (LOFC) #3 data for the 9 MW test case with the vessel cooling system (VCS) off were made available through the Nuclear Energy Agency LOFC project framework. The neutronic model developed for the initial test (LOFC#1) achieved a satisfactory level of maturity, demonstrating its accuracy in predicting power evolution and core recriticality. However, the LOFC#3 should be used to primarily investigate thermal hydraulic phenomena, as the reactor was shut down prematurely due to overheating in the upper reactor components, which prevented re-criticality.

This report focuses on advancing the HTTR thermal hydraulic model to accurately simulate the LOFC#3 scenario. The work includes simulating the LOFC#3 benchmark and generating the corresponding benchmark specifications. These efforts aim to ensure consistency across participant models and provide essential data for future participants, including private industry stakeholders seeking to validate their computational tools.

Page intentionally left blank

CONTENTS

ABSTRACT	v
ACRONYMS	xi
1. NEED FOR AN HTTR BENCHMARK	1
1.1. Review of LOFC Physics Without Scram	1
2. DEVELOPMENT OF THE HTTR BENCHMARK	2
2.1. HTTR Geometry Specification	3
2.2. Material Specifications	3
2.2.1. Specification of Neutronics Materials	3
2.2.2. Specification of Material Thermal Properties	5
2.3. Benchmark Procedures	5
2.4. Benchmark Figures of Merit	6
3. OVERVIEW OF THE LOFC TEST 3	6
3.1. VCS Description	6
4. DEVELOPMENT OF A PRONGHORN MODEL OF HTTR	8
5. PRONGHORN MODEL OF THE LOFC#3	13
5.1. LOFC#3 Without PHPS Flow	13
5.2. LOFC#3 with PHPS Flow	15
5.3. LOFC#3 Model Conclusions	17
6. CONCLUSIONS	17
7. REFERENCES	18

FIGURES

Figure 1.	UO ₂ thermal conductivity for Tests 1 and 3.	5
Figure 2.	Core layout of the HTTR.....	8
Figure 3.	Zoomed-in view of the fuel and coolant channel.	9
Figure 4.	Block temperature distribution predicted by Pronghorn in a full-power steady state.	11
Figure 5.	Helium temperature distribution predicted by Pronghorn in a full-power steady state.	12
Figure 6.	Maximum and average fuel block temperature predicted by Pronghorn.	14
Figure 7.	Predicted coolant outlet temperatures.	14
Figure 8.	Side-averaged inner reflector temperature predicted by Pronghorn.	15
Figure 9.	Comparison of coolant outlet temperature with and without the primary helium purification system (PHPS).....	16
Figure 10.	Block maximum and average temperatures with and without the PHPS.	16
Figure 11.	Comparison of permanent side reflector (PSR) inner surface temperature with and without the PHPS flow.	17

TABLES

Table 1. Overview of HTTR design parameters. Rows with a slash indicate low/high temperature operation values.....	1
Table 2. Control rod system information.....	4
Table 3. Material impurity contents.....	4
Table 4. Sample figure of merit (FOM) table.....	6
Table 5. VCS design parameters per train.....	7
Table 6. LOFC#3 initial conditions.....	13
Table 7. LOFC#3 normalized flow rates.....	13

Page intentionally left blank

ACRONYMS

ATWS	anticipated transients without scram
FOM	figure of merit
HTC	heat transfer coefficient
HTGR	high-temperature gas-cooled reactor
HTTR	High Temperature Engineering Test Reactor
JAEA	Japan Atomic Energy Agency
LOFC	loss of forced cooling
MOOSE	Multiphysics Object-Oriented Simulation Environment
PHPS	primary helium purification system
PLOFC	pressurized loss of forced cooling
PSR	permanent side reflector
RPV	reactor pressure vessel
VCS	vessel cooling system

Page intentionally left blank

NEA HTTR LOFC Project Test#3 Benchmark Results

M3AT-24IN0603012

1. NEED FOR AN HTTR BENCHMARK

The High Temperature Engineering Test Reactor (HTTR) is a 30 MW prismatic block gas-cooled reactor built by the Japan Atomic Energy Agency (JAEA) to demonstrate operations and inherent safety of high-temperature gas-cooled reactors (HTGRs). An overview of key HTTR design parameters can be seen in Table 1. Several references exist that provide information about the design of HTTR [1–5]. These resources, in particular [1] and [3], provide detailed geometric and material definitions. Bess [3] notes some discrepancies in reported parameter values, such as burnable poison composition among several sources. Additionally, some parameters, such as the thickness of the side shielding blocks or the size of coolant channels in the blocks between the lower reflector and hot plenum, are not provided in any publications. To provide a pathway for comparing models that are consistent with one another, we have begun the process of developing a benchmark based on HTTR loss of forced cooling (LOFC) tests.

HTTR has been used in three LOFC tests to demonstrate the inherent safety of HTGRs. The first of these tests is referred to as Test 1 and was run in December, 2010 [2]. Test 1 was a LOFC without scram conducted from 30% power (9 MW). The results of Test 1 and a JAEA model of the test were published in Reference [6]. Test 1 is the only test with published results at this point. Test 2 was performed in 2024. This test was a LOFC from 100% power (30 MW) without scram [2]. Test 3 represents a LOFC from 30% power (9 MW) but with the vessel cooling system (VCS) inactive. The VCS, which will be described in further detail later, is an active cooling system that sits outside the vessel and cools both the vessel and concrete of the reactor building. An HTTR benchmark provides value for the HTGR community because several vendors are seeking to deploy prismatic HTGRs. HTTR is the only operating prismatic HTGR. This means the LOFC tests at HTTR can be used to provide validation data for reactor designers, national laboratories, universities, and regulators investigating prismatic HTGRs. A common set of problems and figures of merit with data provides an opportunity for validation studies and an opportunity to assess how modeling decisions and assumptions from one model or code to another impact results. The HTGR thermal hydraulics benchmark provides an opportunity for standalone thermal hydraulics code validation from an integral-effects test facility [7], but HTTR is the only currently operating source of prismatic HTGR multiphysics validation data.

1.1. Review Of LOFC Physics Without Scram

The LOFC is any transient in which forced circulation of the coolant stops. The LOFC comes in two varieties. In the pressurized loss of forced cooling (PLOFC), the coolant pressure boundary remains intact but

Table 1. Overview of HTTR design parameters. Rows with a slash indicate low/high temperature operation values.

Design Parameter	Value
Thermal Power (MW)	30
Coolant Inlet Temperature (K)	668
Coolant Outlet Temperature (K)	1,123/1,223
Coolant Flow Rate $\frac{kg}{s}$	12.4/10.2
Average Power Density $\frac{MW}{m^3}$	2.5
Rated Pressure (MPa)	4.0

forced flow of coolant stops. During this transient, intracore natural circulation flow patterns may develop. The depressurized loss of forced cooling occurs when the coolant pressure boundary is ruptured. During this transient, helium escapes from the primary coolant system and enters containment. This transient can lead to varying degrees of air ingress, creating concerns not just of fuel overheating but also of graphite oxidation. The LOFC tests at HTTR are PLOFCs. Following the onset of a PLOFC, the reactor protection system should trip and shut down the reactor, but the inherent safety characteristics of HTGRs mean that, in the event the reactor protection system fails to activate, fuel can be sufficiently cooled through natural phenomena that there is no concern of radionuclide release to the public.

When forced circulation of helium stops, the fuel and graphite block temperatures rise. The negative fuel and moderator temperature coefficients associated with HTGRs lead to an insertion of negative reactivity that shuts down the fission chain reaction, bringing the reactor to nearly decay heat mode. Fuel temperatures drop relatively quickly after the chain reaction stops, inserting some positive reactivity, but block temperatures continue to rise, inserting more negative reactivity [8]. In addition to the temperature reactivity feedback, the end of the chain reaction leads to an increase in Xe-135 population, as I-135 decays into Xe-135 and the Xe-135 removal term from absorption goes to zero. For several hours, Xe-135 continues to build up, but eventually Xe-135 dies away, leading to first an initial large negative reactivity insertion followed by a positive reactivity insertion. The balance of positive reactivity from fuel cooldown and eventual Xe-135 dieaway combined with block heatup leads to an eventual recriticality and eventual stabilization of fission power at a low level [6]. Previous studies [6, 8] have also noted that an accurate prediction of recriticality requires modeling subcritical multiplication. HTTR includes three neutron startup sources. The presence of an external neutron source in a subcritical multiplying medium, such as HTTR following an insertion of negative reactivity, leads to a stable neutron flux. Accurately capturing this stable flux arising from subcritical multiplication is required for accurate predictions of recriticality and the power peak following recriticality.

During these transients, heat can no longer be removed from the reactor by convection. In the PLOFC, natural circulation flow patterns may develop. These flow patterns can redistribute heat within the reactor, but natural circulation in HTGRs occurs in closed loops within the reactor vessel, so it does not remove heat from the vessel. Heat is removed from the reactor by a combination of conduction and radiation heat transfer. Conduction redistributes heat from the active core to the inner and outer reflectors and the permanent side reflector (PSR). From the PSR, heat radiates to the steel support structures within the reactor pressure vessel (RPV) and to the RPV itself. From the RPV, heat is removed by a system that flows a coolant through a plate that sits somewhere outside the vessel. This system is frequently referred to as the reactor cavity cooling system, but in HTTR, it is referred to as the VCS. The VCS is a system that flows water through steel plates to a heat exchanger that serves as the ultimate heat sink during the LOFC.

2. DEVELOPMENT OF THE HTTR BENCHMARK

A major effort this year has been the development of a first draft of specifications for an HTTR LOFC benchmark. Quality benchmark specifications include either an explicit description of the entire relevant geometry or reference to a document or set of documents that provides that description. A good benchmark will also define material properties to be used—not just the name of the material but actual property values as a function of temperature and other relevant parameters. When isotopic compositions are relevant, such as for any neutronics modeling, benchmark specifications will include atom or weight fractions of each isotope and the physical density to be used in the modeling. Benchmark specifications should also define the procedures for executing the benchmark, particularly for complex multiphysics benchmarks.

2.1. HTTR Geometry Specification

The first aspect of specifications that we developed was the geometry of HTTR. The design of the RPV is detailed by Tachibana et al. [9]. The HTTR LOFC benchmark is intended for intermediate or low-fidelity codes, such as systems codes. As such, detailed geometry information is not strictly necessary. Information such as the total flow area and hydraulic diameter in a given region is often sufficient as opposed to a more detailed resolution of the number and size of coolant channels and their exact positions. Helium enters the vessel at the bottom and rises in the space between the PSR and the side shielding block as well as between the side shielding block and the RPV. The size of the flow channel between the PSR and side shielding block is not published anywhere nor is the size of the gap between the side shielding block and the RPV. Previous Idaho National Laboratory work has used a coupled RELAP5-3D/PHISICS model, and that model was used to determine the flow area and hydraulic diameter of these regions [10]. That model was also used to determine the volume and flow area of the top plenum. We do not present a detailed description of the HTTR geometry in this report, as much of the information on block size and coolant channel layout in the core is widely available [1, 3, 4, 8, 11]. We do, however, discuss details of the geometry that are less discussed but are relevant for capturing the coolant flow and thermal hydraulic behavior of the system.

The geometry of the the upper reflector, core, and top of the lower reflector is well-documented by Bess [3] and the JAEA [1]. In the upper reflector, coolant channels have the same placement as they do in the core, but the diameter of the coolant channels is 23 mm, as opposed to the 41 mm in the core [3, 12]. The geometry of the bottom block of the lower reflector is unclear. It is simply stated that “The bottom replaceable reflector block below each fuel block column provides a transition of the many coolant channels to a single large channel...” [1]; consequently, the area and hydraulic diameter from the RELAP5-3D model used by Lu [10] can be specified for this region. Beneath the bottom lower reflector block are the hot plenum seal and key blocks. The seal block collects coolant from the many blocks below the core and reduces it to a set of seven coolant channels, and the hot plenum key block collects the flow from the seven coolant channels in the seal blocks and combines it to a single channel, thus reducing the number of channels feeding the hot plenum. Detailed geometry of the seal and key blocks is not available, but sufficient information to populate the benchmark specifications for systems code or porous medium models can be extracted from our reference RELAP5-3D model [10].

For the sake of neutronics models, some of the detailed flow geometry described in the previous paragraph is not necessary; however, Bess noted some confusion in the size of the absorber element in the control rods [3]. It is noted in Reference [13] that the absorber element has gaps in it. Based on values reported in References [13] and [14], the control rod information can be seen in Table 2.

2.2. Material Specifications

Defining material properties for a benchmark is essential for both neutronics and thermal hydraulics modeling. In neutronics modeling, defining materials is focused on isotopic compositions (including impurities) and densities. For thermal hydraulics, material properties are generally thermal conductivity, density, specific heat, and emissivity as a function of temperature. It is also common for density and emissivity to be treated as constant values. For this benchmark, material properties are provided in supplemental data files that will be distributed to all participants.

2.2.1. Specification of Neutronics Materials

Specifying neutronics materials consists of defining isotopic abundance ratios and amounts of impurities. Absorber materials in HTTR are composed of a B_4C/C composite with varying ratios of B_4C to C based on the intended absorber (burnable poison or control rod). Different references may provide slightly different

Table 2. Control rod system information.

Parameter	Value
Control Rod Total Length (m)	3.1
Spine/Sleeve Material	Alloy 800H
Spine Diameter (mm)	10
Gap from Spine to Inner Sleeve (mm)	27.5
Inner Sleeve Inner Diameter (mm)	75
Inner Sleeve Outer Diameter (mm)	105
Gap from Absorber to Outer Sleeve (mm)	0.5
Outer Sleeve Thickness (mm)	3.5
Outer Sleeve Outer Diameter (mm)	113.0
Absorber Material	B ₄ C/C Composite, 30 wt% Natural B
Absorber Density ($\frac{g}{cm^3}$)	1.9

abundance ratios for natural boron. For the sake of this benchmark, natural boron should be considered as 18.7 wt% B-10 and 81.3 wt% B-11.

The blocks in HTTR are composed of two varieties of graphite: IG-110 and PGX. The density of IG-110 graphite is defined as $1,770 \frac{kg}{m^3}$, and for PGX graphite, it is $1,780 \frac{kg}{m^3}$. Density values are assumed to be temperature-independent. The impurity content of the graphite material depends on the specific component. The impurity is defined as an equivalent concentration, in parts per million, of natural boron. Material impurity contents, in ppm B equivalent, are defined in Table 3, with values based on Reference [14]. This table quantifies as specific values impurities which are listed in other places as “less than 1 ppm,” or “less than 3 ppm,” etc. The benchmark specifications assign exact values for these impurity contents that are otherwise defined with limits rather than concentrations.

Table 3. Material impurity contents.

Component	Material	Impurity (ppm B equivalent)
Fuel Block	IG-110	1.0
Fuel Compact Sleeve	IG-110	1.0
Fuel Compact	IG-110	1.2
Tristructural Isotropic particle layers	Buffer/PyC/SiC	3.0
Replaceable Reflector Block	IG-110	1.0
Control Rod Guide Block	IG-110	1
Permanent Reflector	PGX	5

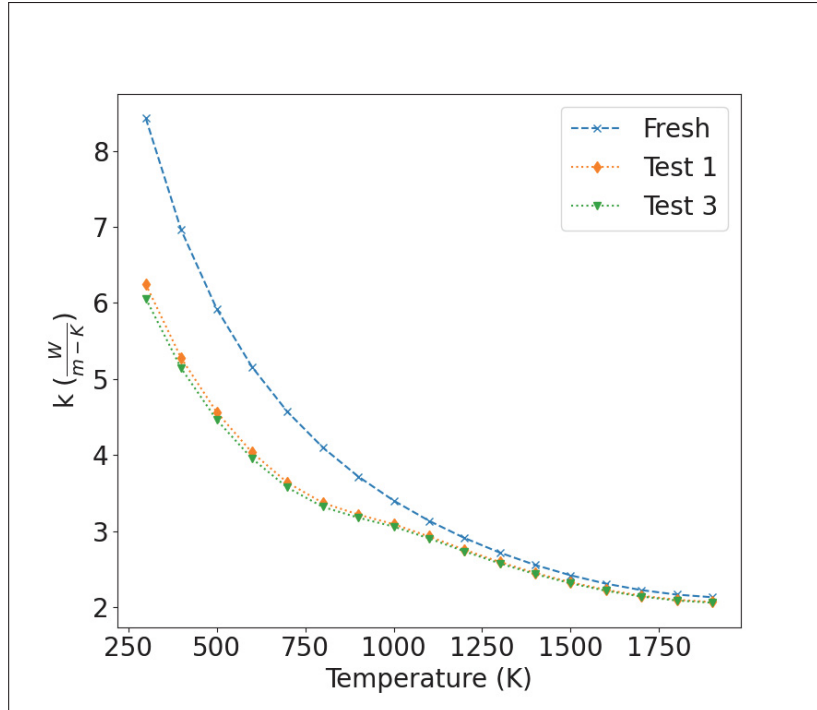


Figure 1. UO_2 thermal conductivity for Tests 1 and 3.

2.2.2. Specification of Material Thermal Properties

Material thermal properties are generally a function of temperature and are often also a function of fluence. The most important materials in HTTR are graphite (mostly IG-110) and UO_2 . Thermophysical properties of all materials are provided in supplementary data tables. Aside from the UO_2 kernel itself, material properties are assumed to be independent of fluence using values provided by JAEA as recommendations. It is common practice to homogenize the thermal properties of the UO_2 , the tristructural isotropic particle layers, and the fuel compact into a single set of properties. This should be done using the property values provided, though we do not specify which approach should be used to homogenize properties. The set of thermal properties has been developed for Tests 1 and 3, but not for Test 2, as Test 2 was the latest test to occur. The burnup of HTTR is quite low, but a strong impact of burnup on UO_2 thermal conductivity can still be seen in Figure 1. The UO_2 has a density of $10.41 \frac{\text{g}}{\text{cm}^3}$. Thermal properties of UO_2 were calculated based on relationships in [15], and below 773 K, the correlations were extrapolated. The extrapolated correlation agreed well with values reported in [16].

Properties of the particle layers were not provided by JAEA and were calculated based on relationships identified in References [17, 18].

2.3. Benchmark Procedures

The benchmark will include three problems, each representing one of the LOFC tests. Each problem will include a steady-state solution and a transient solution. This is a multiphysics benchmark that includes both neutronics and thermal hydraulics modeling. For participants interested in calculating their own power distributions, decay heat curves, cross sections, and Xe-135 reactivity worth, simplified operational histories that preserve burnup will be provided. For participants not interested in calculating their own reactor physics parameters, we will provide reference values from Multiphysics Object-Oriented Simulation Environment (MOOSE) based modeling. The benchmark specifications provide boundary conditions for steady-state

modeling, including the magnitude of the power, the coolant flow rate, the inlet temperature, and the coolant pressure. We provide flow rate and inlet temperature boundary conditions for the VCS as well. The steady-state exercise is used to generate the initial conditions for the transient portion of the problem.

The transient exercise defines a primary coolant flow rate coast-down table. In all three LOFCs, the primary helium purification system (PHPS) was running and providing a small coolant flow rate. Helium flow rate from the PHPS to the core is provided for each problem in a supplemental data file. The inclusion of this flow rate is important, because the small—but still present—forced helium flow rate may inhibit the development of natural circulation, and it may provide some heat removal. Each transient exercise specifies the problem time that the simulation should run to. Problems 1 and 3 both include 18 hours of transient time. The specifications for Problem 2 have not been developed yet, because LOFC#2 was only recently completed.

2.4. Benchmark Figures Of Merit

The benchmark requests figure of merits (FOMs) during both the steady state and transient. Some FOMs are scalar values, and some are time-series values. Each FOM is assessed as to whether it has experimental data it can be directly compared against. If it does, it is considered a validation FOM. Units and precision for each FOM are included as part of the specifications. Table 4 includes a sample of the FOMs requested as part of the benchmark. Coolant flow rate in each region of the core is also considered as a FOM to assess whether or not natural circulation flow is established.

Table 4. Sample FOM table.

FOM	Time Series (TS) or Scalar (S)	Precision	Validation?
Steady-State k_{eff}	S	1 pcm	Yes
Fission Power (MW)	TS	3 significant figures	Yes
Time of Recriticality (min)	S	1 minute	No
Time of First Power Peak (min)	S	1 minutes	Yes
Magnitude of First Power Peak (kW)	S	1 kW	Yes
VCS Outlet Temperature (K)	TS	1 K	Yes
PSR Inner Surface Temperature (K)	TS	1 K	Yes

3. OVERVIEW OF THE LOFC TEST 3

LOFC#3 is an anticipated transients without scram (ATWS) test during which the VCS is also shut down. This test is started from an initial power of 9 MWt. This test is intended to represent a severe accident in which the LOFC occurs and there is no functioning system for active decay heat removal. This test was conducted on January 28, 2022. LOFC#1 ran for 12 hours, but this test ran for just 155 minutes, because VCS pipes reached their temperature limits due to heating by radiation from the RPV.

3.1. VCS Description

The VCS is not active in LOFC#3, but its temperatures do cause the test to be terminated early, so it bears further description. The VCS sits just outside the concrete radiation shield and serves to cool the vessel and prevent the concrete shield from overheating. Kunitomi et al. [19] provide a good representation of the VCS

Table 5. VCS design parameters per train.

Design parameter	Value
Number of Cooling Tubes in Upper Panel	48
Cooling Tube Outer Diameter in Upper Panel (mm)	15.9
Cooling Tube Thickness in Upper Panel (mm)	3.2
Upper Panel Coolant Flow Rate (kg/s)	0.905
Number of Cooling Tubes in Side Panels	108
Cooling Tube Outer Diameter in Side and Bottom Panels (mm)	25.4
Cooling Tube Thickness in Side and Bottom Panels (mm)	3.5
Side Panel Coolant Flow Rate (kg/s)	20.0
Number of Cooling Tubes in Side Part of Lower Panel	96
Number of Cooling Tubes in Lower Panel Bottom	8
Lower Panel (upper part) Total Coolant Flow Rate (kg/s)	0.905

in their Figure 4. The VCS consists of three sets of panels: the upper, side, and lower cooling panels. Each panel consists of two sets or “trains” of the VCS. The two trains operate independently from one another. The VCS consists of a carbon steel panel facing the RPV with small channels that allow water to flow through it. This panel is referred to as the heat removal adjustment panel. This panel was intended as a backup in the event that the heat removal through the nominal VCS panels was insufficient to keep the reactor within safety limits; however, the heat removal adjustment panels never have any water flow through them, because the VCS is capable of removing sufficient heat without the heat removal adjustment panels. Behind these panels are two stainless steel thermally reflecting plates. These plates are intended to prevent overcooling during steady-state operation. Behind the thermally reflecting plates are the actual VCS panels. These panels consist of sets of water cooling tubes arranged in parallel and connected by carbon steel fins. The tubes are arranged in an alternating A-B pattern such that each tube sits next to tubes from the opposite train. Major VCS parameters can be seen in Table 5. Cooling tube thickness is defined as the difference between the outer and inner radius of the steel tube.

The VCS is required to remove at least 0.3 MW per train during full-power operation, and it achieves this function without running any water through the heat removal adjustment panels. During LOFC#3, not only are the pumps running the VCS shut off but valves in the VCS were closed, inhibiting flow through the system through natural circulation.

4. DEVELOPMENT OF A PRONGHORN MODEL OF HTTR

The detailed description of HTTR assembled for the benchmark specifications from several references [1, 3, 4, 14] was used to build a model of the core of HTTR in Pronghorn [20]. This model is a simplified RZ representation of HTTR bounded by the PSR. This model divides the core into a set of concentric rings. Figure 2 shows the core layout. Thick purple lines represent the boundaries used to define the different rings in the model. The region in navy blue bounded inside by purple lines is the PSR. The rings for the RZ model

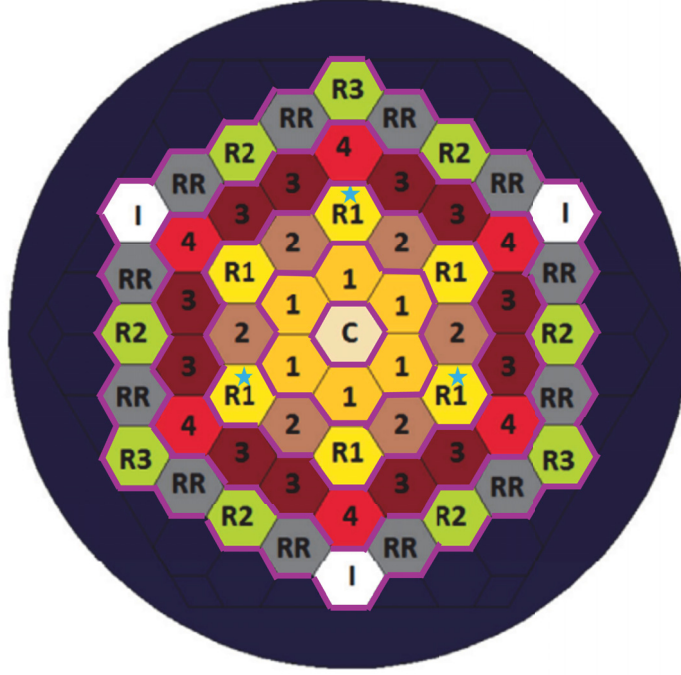


Figure 2. Core layout of the HTTR.

were defined with an area equal to the sum of the total area of the hexagonal blocks. For example, the inner reflector is a circle with an area equal to the area of one hexagonal block, and Ring 1 is an annulus with an inner radius equal to the radius of the inner reflector and an outer radius such that the area of Ring 1 is equal to the area of six hexagonal blocks. The hexagonal blocks have a flat-to-flat distance of 36 cm [14], which means the apothem is 18 cm. The area of a block is given by Equation 1, where A is the area and y is the apothem, or half of the block flat-to-flat distance:

$$A = 6 \times \frac{y^2}{\tan(\frac{\pi}{3})} \quad (1)$$

The radius of the equivalent circle can be found by setting Equation 1 equal to the area of a circle and solving for the radius:

$$6 \times \frac{y^2}{\tan(\frac{\pi}{3})} = \pi r^2 \quad (2)$$

$$r = \sqrt{\frac{6y^2}{\pi \tan(\frac{\pi}{3})}} \approx 1.05y \quad (3)$$

Equations 1–3 hold for a single hexagonal block. To find the outer radius of Ring 1, the area of the hexagons can be converted into an equivalent area of an annulus, or the total area of the inner reflector and Ring 1 can

be found by multiplying Equation 1 by seven (as there are six blocks in Ring 1 and one block in the inner reflector) and solving for the radius from the area. This approach is used to find the outer radius of each ring up to and including the outer reflector. These areas are the total area of the hexagonal block, including both solid and coolant channel area. The radius of the permanent reflector is specified as 2.15 m based on the RELAP5-3D model in Reference [10]. The Pronghorn model uses the outer radius of the PSR as its outer boundary radially. This temperature boundary condition applied outside the PSR is the reactor coolant inlet temperature.

Starting from the top, the HTTR geometry consists of the upper plenum, two upper reflector blocks, five fuel blocks, two lower reflector blocks, the hot plenum seal block, the hot plenum key block, and the hot plenum. In HTTR, the coolant exits the hot plenum through a single pipe at the center of the plenum, allowing coolant to mix in the other regions of the plenum.

The porous medium capabilities of Pronghorn were used in this model. Within each ring, the porosity was calculated based on the coolant volume fraction in each block. Control rod blocks contain three channels, but the coolant flow area in the RELAP5-3D model had just two of those channels available for flow, so we used a porosity assuming just two of the coolant channels were available for flow. The fueled blocks in HTTR have channels containing fuel compacts and coolant flow paths. This can be seen in Figure 3. The porosity calculation treats the fuel compact as solid, so only the yellow region identified as the helium flow channel is considered for the porosity. The same approach was used to determine the flow area of the seal and key blocks beneath the lower reflector. The length of these blocks was provided by JAEA.

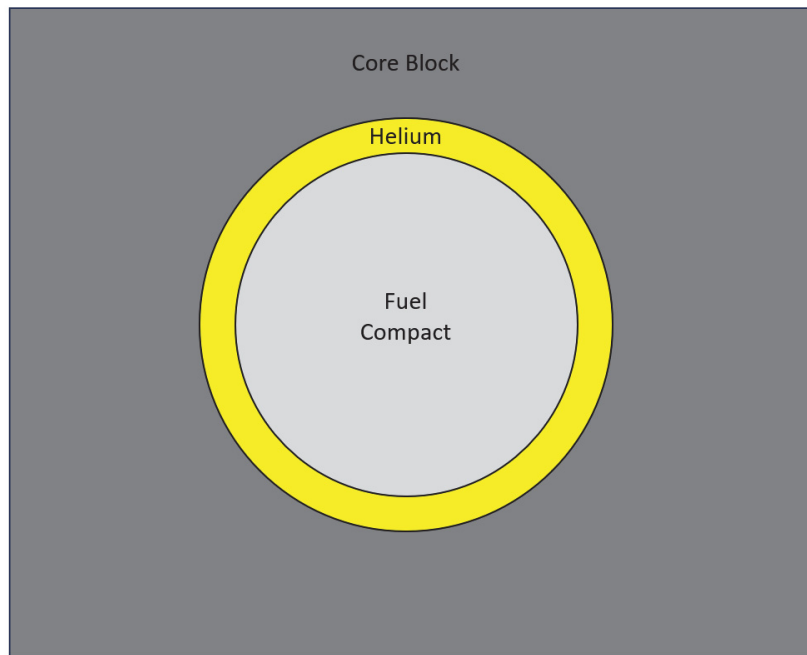


Figure 3. Zoomed-in view of the fuel and coolant channel.

The model we developed is purely a thermal hydraulics model. To determine the axial power distribution, we used the multiphysics model from Laboure et al. [8], which is available on the Idaho National Laboratory Virtual Test Bed [21]. The axial power distribution from that model was extracted and fit to a Gaussian function that was applied to the fueled blocks. Results reported by JAEA showed that the power density radially was relatively flat [22], so we used the same power density in Rings 1 and 3. Ring 2 had just half the power density of Rings 1 and 3, because Ring 2 is composed of equal parts fuel and control rod blocks.

The coolant flow rate was imposed as a fixed-temperature, fixed-velocity boundary condition at the top of the upper plenum, and a fixed-pressure outlet condition was applied at the bottom-left of the lower plenum. The PSR is composed entirely of solid PGX graphite, and no fluid flows there. The side walls of the upper and lower plena have fixed-temperature boundary conditions using the coolant inlet temperature as the temperature. The left-hand side of the model has a zero heat-flux boundary condition due to the symmetry of the problem.

Pronghorn features many correlations for calculating heat transfer coefficient (HTC), but most of them are intended for packed-bed models. Packed-bed correlations are not representative of conditions in HTTR, but Pronghorn does contain the Dittus Boelter correlation, which is widely used for predicting HTC in channel flow scenarios. Pronghorn natively expects a volumetric heat transfer coefficient [$\frac{W}{m^3-K}$], but the Dittus Boelter model in Pronghorn returns an HTC with units of [$\frac{W}{m^2-K}$]. The `FunctorDittusBoelterWallHTC` package in our Pronghorn version was modified to return a volumetric heat transfer coefficient instead, and the modified `FunctorDittusBoelterWallHTC` package was used for heat transfer between the helium and the core blocks. The modification consisted of taking the HTC calculated by `FunctorDittusBoelterWallHTC` and multiplying by $\frac{4}{D_h}$, where D_h is the hydraulic diameter.

We first tested our model using a full-power steady state. Initial predictions from this model used the `FunctorChurchillDragCoefficients` in the core to predict frictional pressure drop, but this led to a flow distribution with most of the flow through the inner and outer reflectors rather than through the core, with 54% of the flow going through the outer reflector. Using that flow distribution, peak block temperatures were reaching temperatures as high as 1,900 K. We know that temperature is too high, because HTTR design requirements limit the fuel temperature to 1,873 K. Changes in flow area introduce pressure drops, sometimes called minor losses or form losses. These losses depend on the ratio of small-to-large flow areas. Pronghorn does not natively calculate these minor losses. The `FunctorConcentratedLossDragCoefficient` capability allows users to input a form loss coefficient that applies the pressure drop over some small length. When we calculated form losses and used those at area changes in the model, the flow distribution changed, leading to a distribution with 71% of the flow going through the fueled blocks. This distribution is better, but we have little information available to determine the actual flow distribution in the core.

We calculated form losses using the following relationships, where equation 4 is used when the flow area is contracting and equation 4 is used when the flow area is expanding. These losses were applied, with appropriate values for each ring, at the boundary between the upper plenum and the upper reflector, the boundary between the upper reflector and fuel blocks, the boundary between the lower reflector and fuel blocks, and the boundary between the lower reflector and the two hot plenum blocks.

$$K = 0.5 \times \left(1 - \frac{A_1}{A_2}\right)^{0.75} \quad (4)$$

$$K = \left(1 - \frac{A_2}{A_1}\right)^2 \quad (5)$$

When we use the Churchill drag coefficients to calculate friction in the core, we get a pressure drop of 4.13 kPa. When we use the form losses, we still include the Churchill coefficients, but we reduce them to one one-thousandth of their normal value to make the pressure drop primarily a function of the form loss coefficients. When the reduced Churchill coefficients are used in combination with the form loss coefficients, the pressure drop is 3.91 kPa. Choosing not to reduce the Churchill coefficients when using the form loss coefficients also leads to a pressure drop of 3.91 kPa. Both approaches (Standalone Churchill friction and form loss with reduced Churchill) show pressure drops that are significantly lower than the pressure drop measured in the steady state prior to the onset of LOFC 2. The pressure drop predicted by the RELAP5-3D

model from Lu et al. [10] predicts a pressure drop of 5.55 kPa, which is approximately 60 % of the measured pressure drop. The values predicted by Pronghorn are less than half of the measured pressure drop. Further studies are required to determine the correct flow distribution, and coupling this Pronghorn model with a Griffin model to generate new power distributions will also change the flow distribution. We can potentially validate the flow distribution by comparing temperatures at the entrance to the hot plenum in the Pronghorn model to temperatures measured in HTTR at that location, but that analysis is not part of this work. The distributions of fuel and block temperatures can be seen in Figures 4 and 5.

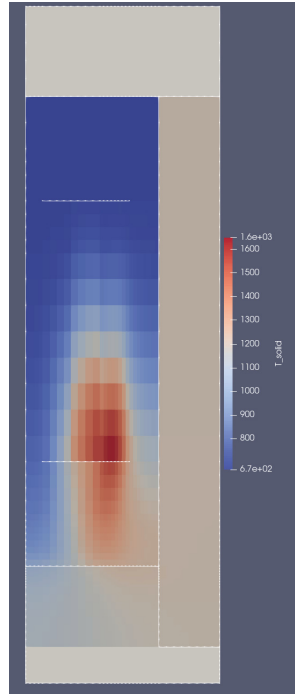


Figure 4. Block temperature distribution predicted by Pronghorn in a full-power steady state.

We have developed an RZ porous medium model of HTTR in Pronghorn. We had to modify the Dittus Boelter calculations in Pronghorn to return a volumetric HTC as opposed to a normal HTC to predict block-to-coolant heat transfer. We initially predicted block temperatures that could exceed the maximum fuel temperature limit, but upon implementing form losses using the `FunctorConcentratedDragLossCoefficient` capability, we predicted block temperatures below the maximum fuel temperature limit at full-power steady state. This is a purely thermal hydraulics model, with a fixed power distribution derived from previous HTTR modeling and literature [8, 22]. The model does not include anything beyond the outer edge of the PSR. Expanding this to a model that includes the entirety of the vessel and possibly the VCS is an area of future work, as is coupling this model to Griffin and other MOOSE apps. The results presented in this work are preliminary, and further work is planned to gain more insight into the mass flow distribution and to better predict the pressure drop. We intend to build upon and improve this model for future HTTR validation work.

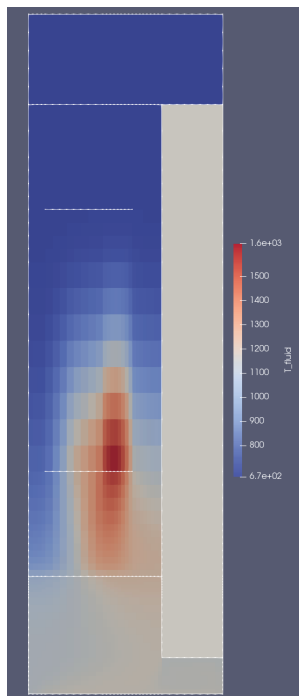


Figure 5. Helium temperature distribution predicted by Pronghorn in a full-power steady state.

5. PRONGHORN MODEL OF THE LOFC#3

Using the Pronghorn model we developed, we implemented boundary conditions representative of LOFC#3. Those boundary conditions are shown in Table 6. The experiment for LOFC#3 was stopped at 155 minutes, which is well before recriticality would be expected to occur. As a result of this, rather than coupling this model to a Griffin model, we used the decay heat curve from Laboure et al. [8] and ran our LOFC model for just 3 hours. In the previous section, we highlighted some areas where the performance of our model could be improved, such as in prediction of mass flow distribution and pressure drop; thus, these should be considered preliminary results for LOFC#3.

Table 6. LOFC#3 initial conditions.

Parameter	Value
Total Power (MW)	9
Coolant Inlet Temperature (K)	454
Coolant Flow Rate (kg/s)	11.4
Pressure (MPa)	2.83

5.1. LOFC#3 Without PHPS Flow

Following the loss of flow, the insertion of positive reactivity should cause the reactor to enter decay heat mode. This model does not capture the initial temperature rise that would insert the reactivity required to bring the reactor to decay heat mode. We make the simplifying assumption, absent an ability to predict reactivity in this model, that the reactor immediately enters decay heat mode. The normalized flow rate versus time used in this model can be seen in Table 7. These values are based on helium flow rates measured in the primary loop. There is no direct flow rate measurement within the core.

The maximum and average fuel block temperatures predicted by Pronghorn can be seen in Figure 6. The maximum block temperature decreases for the entire 3 hour period, while the average block temperature first decreases due to the decrease in power but then increases due to the loss of flow. There are no measurements of block temperature in the core region to compare temperatures against, but these results are consistent with expected system behavior.

Table 7. LOFC#3 normalized flow rates

Time (minutes)	Normalized Flow (-)
0.0	1.000
1.0	0.603
2.0	0.008
3.0	0.0

Helium outlet temperatures are measured by 21 thermocouples. Three of these thermocouples are located near the center of the facility, and the remainder are located at a point further out. We calculated the helium exit temperature from the inner reflector blocks and at a point that approximately corresponds with the outer core thermocouples. In steady state, the temperature of the inner core thermocouples is 574 K, which is about 25 K lower than the average measured temperature. In the outer core regions, the temperature we calculated was 620 K, which is about 30 K higher than the average measured value. These differences suggest that we have not accurately captured the flow rate in the experiment; however, the differences are not so drastic as to make this analysis meaningless. The predicted coolant outlet temperatures over time can be seen in Figure 7.

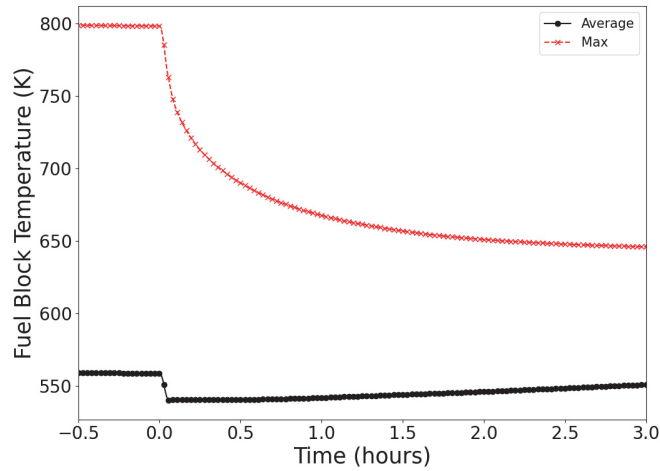


Figure 6. Maximum and average fuel block temperature predicted by Pronghorn.

The LOFC#3 data indicate a small initial rise in temperature followed by a long-term decrease. Pronghorn predicts a rapid initial decrease as the reactor shuts down and flow coasts down, but that is followed by a long-term heatup. The initial rapid cooldown is not present in the data, but it is present in the model. This may be a result of the flow coast down we used. This may be because the model we used assumed the power dropped immediately upon the onset of the LOFC. In reality, the power will not drop until the fuel and block temperature rise slightly. This temperature rise will then propagate to the helium. Our standalone Pronghorn model does not include the effects of reactivity feedback, so we assumed the power dropped instantly. This is likely the cause for the significant differences between model and data. This model also did not include flow from the PHPS, because over the 3 hours from this test, we were not expecting to see the development of stable natural circulation flow patterns, even under ideal conditions for natural circulation.

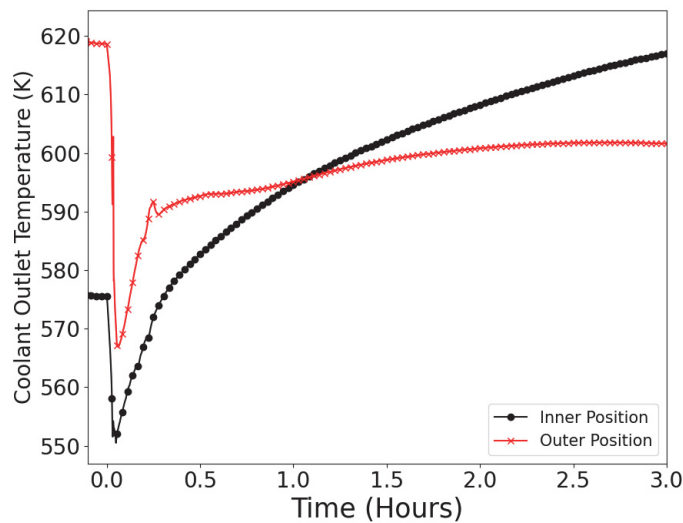


Figure 7. Predicted coolant outlet temperatures.

The measured temperatures closest to the core are the temperatures on the inner surface of the PSR. We compared the side-averaged temperature of the inner surface of the PSR to the average value of all nine PSR thermocouples. We found that in steady state, our PSR temperature was just over 100 K too high. Overpredicting this temperature is not especially surprising, given that Section 4 highlighted that the coolant outlet temperatures near the outer part of the core were too low compared to data. Figure 8 shows the temperature predictions over time for the test. The temperature initially experiences a sharp rise in the first several minutes followed by a more gradual rise. The total temperature rise is 11 K. Though seemingly slight, this is significantly higher than the temperature rise experienced by the inner surface of the PSR during LOFC#3. Both the model and the experiment show a temperature rise, but the experimental temperature rise is much lower than the one predicted by the model.

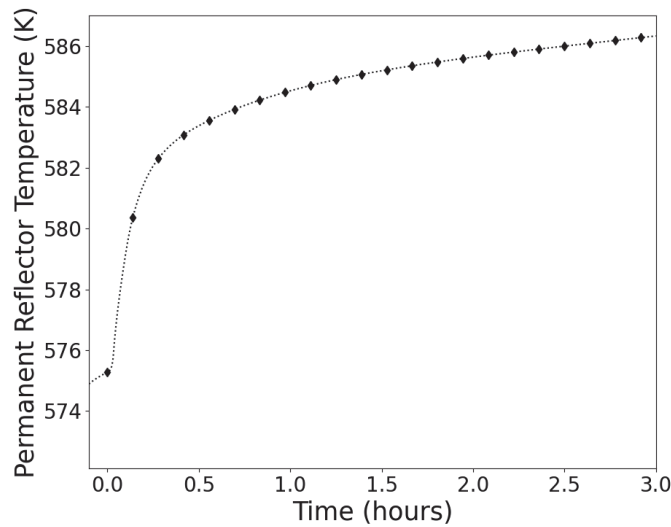


Figure 8. Side-averaged inner reflector temperature predicted by Pronghorn.

These results suggest that the model requires further development. We also decided to test the model under conditions with PHPS flow to see how the results changed.

5.2. LOFC#3 With PHPS Flow

The flow rate through the PHPS is small, but it does decrease slightly over time. Rather than implementing a time-varying PHPS flow rate, we chose to use the average value of the flow rate over time, which is 18 g/s. Perhaps more significant on the results than the exact flow rate of the PHPS is the PHPS inlet temperature. Helium entering the core from the PHPS enters at a temperature of 294 K. This is significantly lower than any other temperature in HTTR at the onset of the LOFC.

Figure 9 shows the impact of the PHPS on coolant outlet temperature. Temperatures in the inner reflector region are lower, but temperatures in the outer reflector region are higher. This is likely a result of energy being removed from the outer core by the PHPS flow. Coolant temperatures still exhibit an initial drop followed by a long-term rise, suggesting that there may be need to revisit the flow coast-down curve. Based purely on coolant outlet temperature, it is difficult to ascertain whether including PHPS flow improves the performance of the model.

A comparison of maximum and average fuel block temperatures with and without the PHPS flow shows that even the small flow rate of 18 g/s introduces a noticeable amount of energy removal from the blocks.

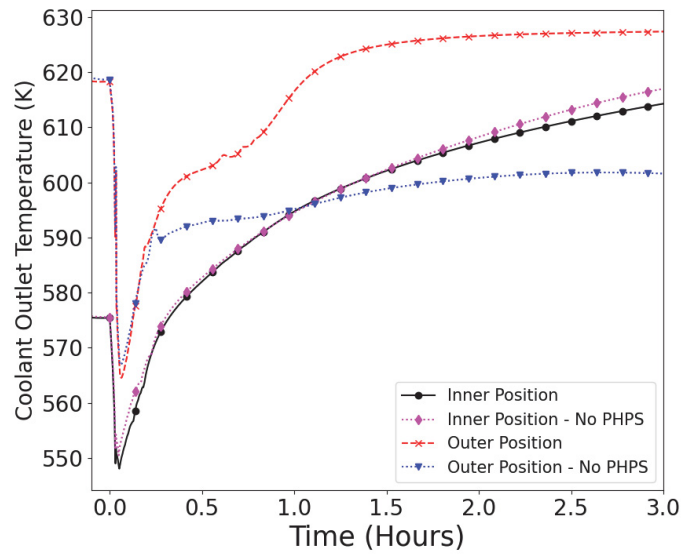


Figure 9. Comparison of coolant outlet temperature with and without the PHPS.

Both peak and average block temperatures are lower when the PHPS is running, as shown in Figure 10. This result suggests that including the PHPS flow may be important in all HTTR transient modeling.

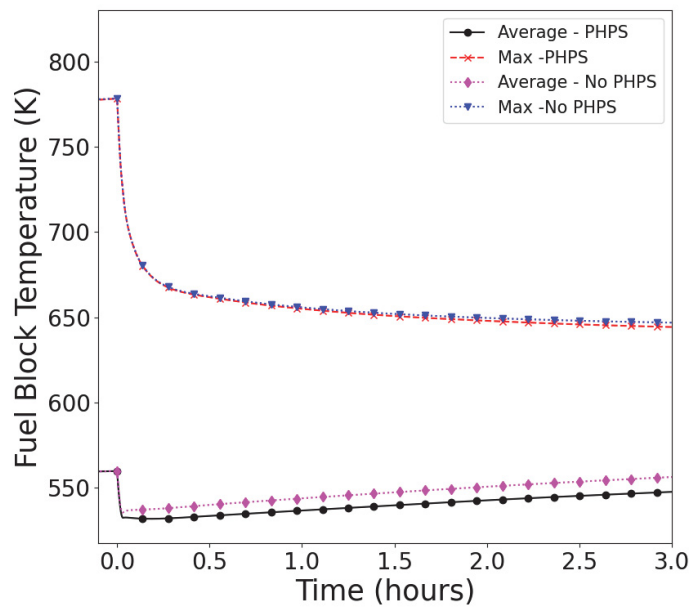


Figure 10. Block maximum and average temperatures with and without the PHPS.

Figure 10 shows that the PHPS removes a non-negligible amount of heat during the beginning of the LOFC, but it does not constitute improvement in the model behavior because it cannot be compared to data. On the other hand, Figure 11 shows that including the PHPS flow leads to a reduction in the PSR temperature

rise and even a temperature drop. This strongly suggests that including the PHPS flow is an improvement in the performance of the model, though the temperature rise in the PSR is still much too great.

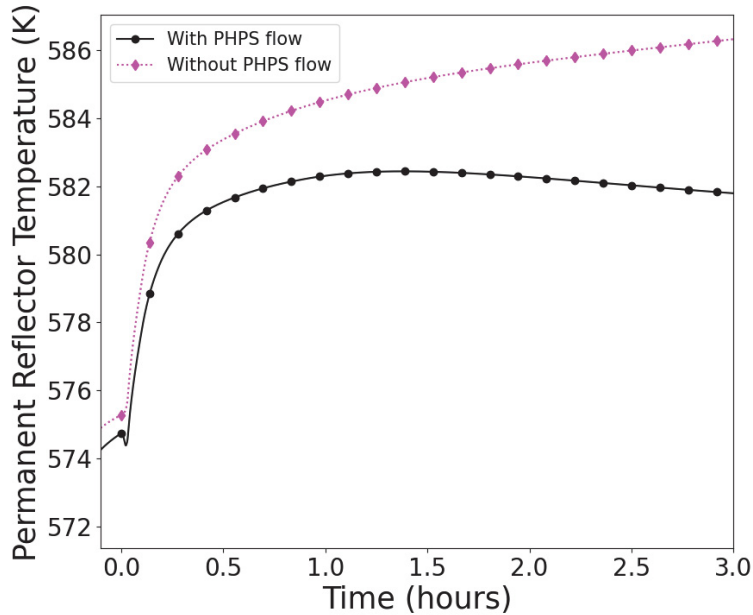


Figure 11. Comparison of PSR inner surface temperature with and without the PHPS flow.

5.3. LOFC#3 Model Conclusions

Both models show a temperature rise in the PSR that is about 10 K too high compared to the data. Including the PHPS flow had a noticeable impact on the prediction of PSR temperature, but it was insufficient to bring the temperature rise to the measured value. Including the PHPS flow did not change the trends in coolant outlet temperature, but it did make the prediction of outlet temperature in the outer regions worse. The incorrect shape of coolant outlet temperature versus time is likely a result of the flow coast-down curve implemented in the Pronghorn model. Future work should look at implementing reactivity feedback to see how more accurately capturing the power behavior impacts the temperature behavior.

6. CONCLUSIONS

In this report, we have presented the need for a unified HTTR benchmark for the LOFC tests. These are valuable sources of multiphysics data for validating HTGR modeling and simulation tools. Providing a single set of boundary conditions and some required geometry for the system ensures we can compare predictions of temperature and power consistently among several HTTR models. We further discussed our efforts to develop a benchmark for the three LOFC tests. We have drafted benchmark specifications and provided them for review to JAEA and the Organization for Economic Cooperation and Development's Nuclear Energy Agency for their review and received positive feedback. Benchmark specifications still need to be finalized, particularly given how recently the LOFC#2 test was performed.

We developed a Pronghorn model of HTTR and provided some preliminary results. Our analysis of steady state at both 30 MW and 9 MW indicates that the flow distribution is likely incorrect in the model.

Our analysis of the LOFC#3 test showed a reflector temperature rise that was far too high, and the shape of temperature versus time for coolant outlet temperature was incorrect. We hypothesize that the latter result is due to an incorrect flow coast-down curve and suggest that future work look at a more rapid coast down. We saw that including the small flow from the PHPS led to an improvement in the prediction of PSR temperature, but it was not sufficient to bring the temperature rise to within expected values. More work is needed to improve the performance of this model, including coupling with other MOOSE apps to capture the multiphysics behavior of the core and expanding the model to include the helium riser, core barrel, and VCS.

7. REFERENCES

- [1] Saito, S., Tanaka, T., and Sudo, Y., Design of high temperature engineering test reactor (HTTR). Technical report, Japan Atomic Energy Research Inst. (1994).
- [2] Nagatsuk, K., Noguchi, H., Nagasumi, S., Nomoto, Y., Shimizu, A., Hiroyuki, S., Nishihara, t., and Sakaba, N. (2024) Current status of high temperature gas-cooled reactor development in Japan. *Nuclear Engineering and Design*, **425**, 113338.
- [3] Bess, J. D. and Fujimoto, N., Evaluation of the Start-up Core Physics Tests at Japan's High Temperature Engineering Test Reactor (Fully-Loaded Core). Technical Report NEA/NSC/DOC(2006)1, Organization for Economic Cooperation and Development, Nuclear Energy Agency (2006).
- [4] Fujiwara, Y., Goto, M., Iigaki, K., T, I., Ho, H. Q., Kawamoto, T., Kondo, M., and Kunitomi, K. e. a. High Temperature Gas-cooled Reactors chapter 2, pp. 17–177 Academic Press (2021).
- [5] Fujiwara, Y., Goto, M., Iigaki, K., T, I., Ho, H. Q., Kawamoto, T., Kondo, M., and Kunitomi, K. e. a. High Temperature Gas-cooled Reactors chapter 2, pp. 257–311 Academic Press (2021).
- [6] Takamatsu, K., Yan, X. L., Nakagawa, S., Sakaba, N., and Kunitomi, K. (2014) Spontaneous stabilization of HTGRs without reactor scram and core cooling - Safety demonstration tests using the HTTR: Loss of reactivity control and core cooling. *Nuclear Engineering and Design*, **271**, 379–3872.
- [7] Epiney, A., Strydom, G., Kile, R., Retamales, M. T., Yoon, S., Mueller, C., Gutowska, I., Zou, L., Hua, T., and Fang, J. (2022) Overview of HTTF Modeling and Benchmark Efforts for Code Validation for Gas-Cooled Reactor Applications. In *Proc. 4th Int. Conf. Generation IV Small Reactors (G4SR-4)* pp. 3–6.
- [8] Labouré, V., Ortensi, J., Martin, N., Balestra, P., Gaston, D., Miao, Y., and Strydom, G. (2023) Improved multiphysics model of the High Temperature Engineering Test Reactor for the simulation of loss-of-forced-cooling experiments. *Annals of Nuclear Energy*, **189**, 109838.
- [9] Tachibana, Y., Nakagawa, S., and Iyoku, T. (2004) Reactor pressure vessel design of the high temperature engineering test reactor. *nuclear engineering and design*, **233**(1-3), 103–112.
- [10] Lu, C. Fully Ceramic Microencapsulated Fuel in High-Temperature Gas-Cooled Reactors PhD thesis The Pennsylvania State University (2019).
- [11] Shiozawa, S., Fujikawa, S., Iyoku, T., Kunitomi, K., and Tachibana, Y. (2004) Overview of HTTR design features. *Nuclear Engineering and Design*, **233**(1-3), 11–21.
- [12] Agency, I. A. E., Evaluation of high temperature gas cooled reactor performance: Benchmark analysis related to initial testing of the HTTR and HTR-10. Technical Report IAEA TECDOC 1382, International Atomic Energy Agency (2003).

- [13] Tachibana, Y., Sawahata, H., Iyoku, T., and Nakazawa, T. (2004) Reactivity control system of the high temperature engineering test reactor. *Nuclear Engineering and Design*, **233**(1-3), 89–101.
- [14] Fujimoto, N., Nojiri, N., Ando, H., and Yamashita, K. (2004) Nuclear design. *Nuclear engineering and design*, **233**(1-3), 23–36.
- [15] Harding, J. and Martin, D. (1989) A recommendation for the thermal conductivity of UO₂. *Journal of nuclear materials*, **166**(3), 223–226.
- [16] Carbajo, J. J., Yoder, G. L., Popov, S. G., and Ivanov, V. K. (2001) A review of the thermophysical properties of MOX and UO₂ fuels. *Journal of Nuclear Materials*, **299**(3), 181–198.
- [17] Snead, L. L., Nozawa, T., Katoh, Y., Byun, T.-S., Kondo, S., and Petti, D. A. (2007) Handbook of SiC properties for fuel performance modeling. *Journal of nuclear materials*, **371**(1-3), 329–377.
- [18] Powers, J. J. and Wirth, B. D. (2010) A review of TRISO fuel performance models. *Journal of Nuclear Materials*, **405**(1), 74–82.
- [19] Kunitomi, K., Nakagawa, S., and Shinozaki, M. (1996) Passive heat removal by vessel cooling system of HTTR during no forced cooling accidents. *Nuclear engineering and design*, **166**(2), 179–190.
- [20] Novak, A., Carlsen, R., Schunert, S., Balestra, P., Reger, D., Slaybaugh, R., and Martineau, R. (2021) Pronghorn: A Multidimensional Coarse-Mesh Application for Advanced Reactor Thermal Hydraulics. *Nuclear Technology*, **207**, 1015–1046.
- [21] Giudicelli, G. L., Abou-Jaoude, A., Novak, A. J., Abdelhameed, A., Balestra, P., Charlot, L., Fang, J., Feng, B., Folk, T., Freile, R., Freyman, T., Gaston, D., Harbour, L., Hua, T., Jiang, W., Martin, N., Miao, Y., Miller, J., Naupa, I., O’Grady, D., Reger, D., Shemon, E., Stauff, N., Tano, M., Terlizzi, S., Walker, S., and Permann, C. (2023) The Virtual Test Bed (VTB) Repository: A Library of Reference Reactor Models Using NEAMS Tools. *Nuclear Science and Engineering*, **0**(0), 1–17.
- [22] Takada, E., Nakagawa, S., Fujimoto, N., and Tochio, D. (2004) Core thermal–hydraulic design. *Nuclear engineering and design*, **233**(1-3), 37–43.